

# Coulomb Interaction-Stabilized Isolated Narrow Bands with Chern Numbers $\mathcal{C} > 1$ in Twisted Rhombohedral Trilayer-Bilayer Graphene

Võ Tiến Phong<sup>1,2,\*</sup> and Cyprian Lewandowski<sup>1,2,†</sup>

<sup>1</sup>*Department of Physics, Florida State University, Tallahassee, FL, 32306, U.S.A.*

<sup>2</sup>*National High Magnetic Field Laboratory, Tallahassee, FL, 32310, U.S.A.*

(Dated: June 13, 2025)

Recently, fractional quantum anomalous Hall effects have been discovered in two-dimensional moiré materials when a topologically nontrivial band with Chern number  $\mathcal{C} = 1$  is partially doped. Remarkably, superlattice Bloch bands can carry higher Chern numbers that defy the Landau-level paradigm and may even host exotic fractionalized states with non-Abelian quasiparticles. Inspired by this exciting possibility, we propose twisted *rhombohedral* trilayer-bilayer graphene at  $\theta \sim 1.2^\circ$  as a field-tunable quantum anomalous Chern insulator that features spectrally-isolated, kinetically-quenched, and topologically-nontrivial bands with  $\mathcal{C} = 2, 3$  favorable for fractional phases once fractionally doped, as characterized by their quantum geometry. Based on extensive self-consistent mean-field calculations, we show that these phases are stabilized by Coulomb interactions and are robust against variations in dielectric environment, tight-binding hopping parameters, and lattice relaxation.

Fractionalized phases that emerge from doping a quantum anomalous Chern insulator are highly-sought after because they may host quasiparticles with non-Abelian exchange statistics, importantly in lattice systems without a magnetic field [1–7]. These exotic quasiparticles are fascinating on their own right [8], but much of the excitement surrounding them concerns their potential application in topological quantum computation [9]. Within the past two years, these fractional Chern insulating (FCI) states have finally been experimentally measured in two classes of materials: twisted MoTe<sub>2</sub> bilayers without displacement field [10–18] and rhombohedral graphene multilayers aligned with hexagonal boron nitride (hBN) with displacement field [19–21]. In twisted MoTe<sub>2</sub>, theoretical calculations suggest that the fractional states emerge from partial filling of a valence band with  $|\mathcal{C}| = 1$  that exists already in non-interacting band structure modeling [22–31]. In rhombohedral graphene-hBN heterostructures, fractional states have only been observed at displacement fields  $\sim 1$  V/nm where the conduction electrons are pushed *away* from the substrate [19–21]. In this regime, the non-interacting conduction bands are essentially those of pristine rhombohedral graphene multilayer with minimal influence from the hBN substrate [32–43]. That is, the conduction band where electrons would populate is nearly dispersionless but it has no discernible gap to the next higher-energy band [44–46]. However, upon including electron-electron interactions, at least at the mean-field level, the narrow band decouples from the other energy bands, generating a mean-field gap  $\sim 10$ – $20$  meV, and carrying a Chern number  $|\mathcal{C}| = 1$  [32–41]. This band remains more or less flat at the mean-field level, and is thus, conducive to further strong interaction effects at partial filling. These graphene-based platforms offer the insight that non-interacting band structures can only predict a subset of possible topological materials that can fractionalize, i.e. they can predict twisted MoTe<sub>2</sub> but not graphene-hBN moiré systems.

Despite their important differences, both aforementioned systems fractionalize from doping  $|\mathcal{C}| = 1$  bands. In principle, superlattice systems can support bands with any in-

teger Chern number [47, 48]. Theories predict that these states are qualitatively much richer than their Landau-level analogues [49–55]. Higher-Chern bands can stabilize fractional states at generalized Jain bosonic and fermionic fillings; these states can be both Abelian and non-Abelian. Therefore, superlattice materials present the exciting possibility of fractionalizing higher-Chern bands without any Landau-level counterpart. Many moiré materials have been proposed to host higher-Chern bands on the basis of non-interacting band structure modeling, including, just to name a few, twisted double bilayer graphene [56–59], twisted AB-ABC graphene [60], helical trilayer graphene and analogues [61–64], buckled bilayer graphene [65, 66], periodically gated multilayer graphene [67–69], and others [70–72]. Various higher-Chern bands have been observed experimentally as well, which however host other (non-FCI) correlated states at fractional fillings of the corresponding higher-Chern bands [73–76]. Despite extensive effort, the experimental observation of fractionalized states emerging from higher-Chern bands remains an unfulfilled aspiration to date.

In this work, we take a step towards making realistic predictions for a material platform that hosts higher-Chern bands endowed with favorable quantum geometry for FCI states. Our system is constructed from rhombohedral graphene multilayers whose conduction bands can be kinetically quenched by a moderate displacement field when the number of layers is large<sup>1</sup>. By bringing a rhombohedral trilayer and bilayer stack together with a relative twist angle, henceforth referred to as twisted rhombohedral multilayer graphene (TRMG<sub>3+2</sub>), we show this system is a suitable candidate for higher-Chern physics. TRMG<sub>3+2</sub> is one member of a broader family of TRMG<sub>M+N</sub> that has been considered in several earlier theoretical works [60, 77–82], wherein it has been shown that

<sup>1</sup> It is a bit subjective what “large” here means. Essentially, what we need is a system that can be made to have a nearly dispersionless conduction band minimum at experimentally-accessible displacement fields. For concreteness, let us just say that large is anything above two layers.

the non-interacting band structures contain higher-Chern narrow bands. On the basis of the chiral model that retains only a minimal set of known hoppings [83, 84], Refs. [78–80] argue that these bands are ideal Chern bands where the Berry curvature and quantum metric exactly satisfy proportionality [85–88]. Building on these works with the insight from graphene-hBN FCI’s deterministic role of Coulomb interactions, we analyze the formation of narrow Chern bands with  $C = 2, 3$  after Hartree-Fock (HF) renormalization. We find that Coulomb interactions are simultaneously crucial to the spectral isolation of these bands from their proximal partners and to the stabilization of their favorable quantum geometry. In the interest of realistic modeling, we include all known hoppings of rhombohedral graphite, account for electrostatic screening from both metallic gates and charge redistribution among the different layers of TRMG<sub>3+2</sub>, and allow for some layer buckling across the twist interface. We find that these post-HF Chern bands are stable in prominent regions of phase space and are robust against changes in dielectric environment and hopping parameters. Therefore, on the basis of our extensive mean-field calculations, we propose TRMG<sub>3+2</sub> as a suitable candidate for the exploration of possible FCI states emerging from a higher-Chern narrow band.

To begin, we construct TRMG<sub>3+2</sub> by stacking Bernal bilayer graphene on top of rhombohedral trilayer graphene with a relative twist angle  $\theta$ . We focus on this combination because both the trilayer and bilayer substacks can be locally gapped by an interlayer displacement field and made to feature spectral regions with high density of states. This feature is crucial for our study as it allows us to tune into different regions in phase space where the interplay between topology and electron-electron interactions is important. TRMG<sub>3+2</sub> is chosen to comprise of different layer numbers so that the competition between disparate layer numbers can be ascertained<sup>2</sup>. Two inequivalent stacking orders are possible depending on whether the *pre-twist* alignment of the trilayer and bilayer are parallel or antiparallel<sup>3</sup>. In the parallel (antiparallel) stacking order, the zone-corner degeneracies carry net chiralities of the same (opposite) sign. The two stacking orders are related to each other by a  $C_{2z}$  rotation of the bilayer. The schematic construction of our system is shown in Fig. 1(a). As we will show,

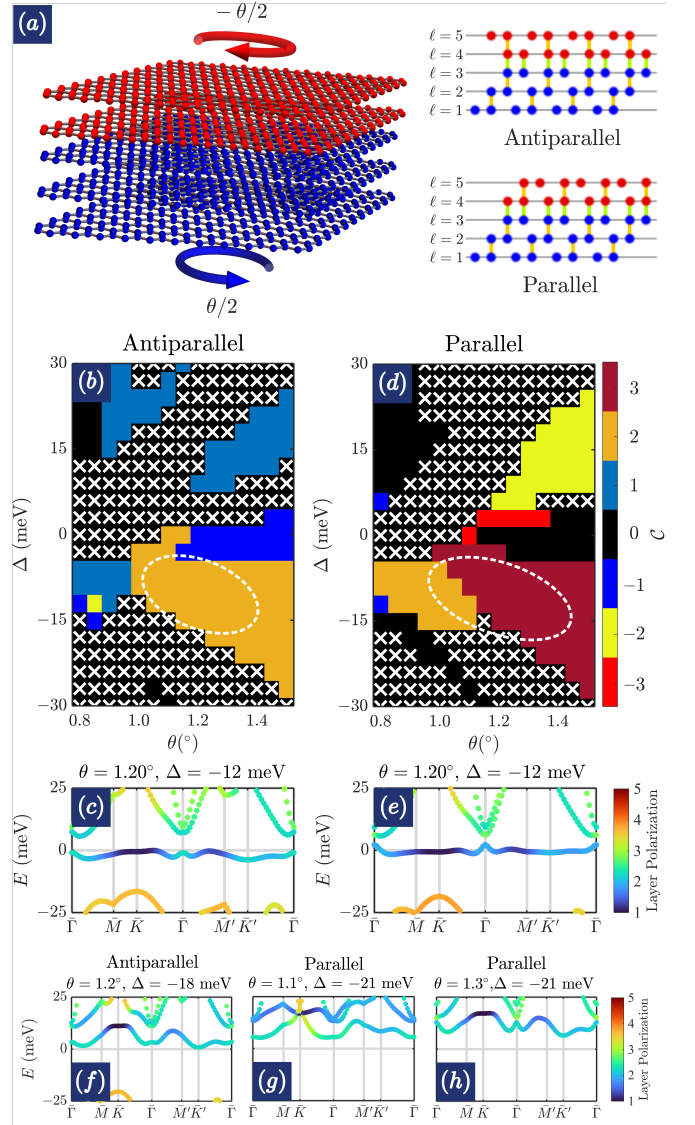


**Figure 1. Moiré heterostructure schematic and topological characterization of the non-interacting band structures.** (a) Construction of a twisted 3 + 2 rhombohedral stack by rotating the bottom trilayer (top bilayer) by  $+\theta/2$  ( $-\theta/2$ ). There are two inequivalent configurations, antiparallel and parallel, depending on the relative stacking orders of the two subsystems. (b) Single-particle (non-interacting) Chern-number characterization of first band above charge neutrality of the antiparallel configuration for values of  $\theta$  and  $\Delta$  where said band is globally isolated.  $\times$  indicates where that band is *not* isolated from the other bands. A dashed line circles the region of interest with  $C = 2$ , reasonably large band gaps, relatively small bandwidths, and small trace condition violations (see discussion in the main text). (c) An example band structure in that region is color coded by layer polarization. (d) Single-particle (non-interacting), Chern-number characterization for the parallel configuration showing a contiguous region featuring  $C = 2$  and  $C = 3$ . A  $C = -2$  phase is also present in this phase diagram, but it does not have the desired spectral properties and quantum geometry. (e) A layer-resolved band structure is shown for a representative point in the dashed circle in (d). (f,g,h) Band structures for values of  $(\theta, \Delta)$  where no clear isolated bands are observed. They are included here for later comparison to HF bands.

<sup>2</sup> Said differently, our choice of 3 + 2 is informed by the following logic. We wish to keep the layer number relatively low for computational speed for this work. So, we fix one of the substacks to be a trilayer because it is the lowest layer number where the rhombohedral nature is evident. The remaining substack can be a monolayer, bilayer, or trilayer. We wish to observe the competition between the two substacks to determine which one, if any, dominates the relevant physics. Therefore, we eliminate the trilayer option. Between the monolayer and bilayer options, we choose the latter since bilayer graphene also locally gaps out in a displacement field.

<sup>3</sup> Concretely, let us label layers  $\ell = 1, 2, 3$  those of the trilayer and layers  $\ell = 4, 5$  those of the bilayer. The twist interface occurs between layers  $\ell = 3, 4$ . The trilayer is oriented in such a way that layer  $\ell + 1$  is shifted by  $+a/\sqrt{3}\hat{y}$  relative to layer  $\ell$ . If the bilayer is oriented the same way, we refer to the stack as parallel. If instead, layer 5 is shifted by  $-a/\sqrt{3}\hat{y}$  relative to layer 4, then we refer to the stack as antiparallel. After alignment, we twist the trilayer by  $+\theta/2$  and the bilayer by  $-\theta/2$ .

these two stacking orders have significantly different mean-field phase diagrams, illustrating the importance of alignment precision. We model the band structure of TRMG<sub>3+2</sub> using a conventional valley-projected continuum approach appropriate for small twist angles [89, 90]:

$$\mathbb{K}_{3+2,\nu} = \begin{pmatrix} \mathbb{K}_{3,\nu}(-i\nabla_{\mathbb{R}-\mathbf{r}}) & \mathbb{T}_{\nu}(\mathbf{r}) \\ \mathbb{T}_{\nu}^{\dagger}(\mathbf{r}) & \mathbb{K}_{2,\nu}(-i\nabla_{\mathbb{R}+\mathbf{r}}) \end{pmatrix} + \mathbb{D}, \quad (1)$$

where  $\mathbb{K}_{3,\nu}$  and  $\mathbb{K}_{2,\nu}$  are the kinetic energy for the rhombohedral trilayer and bilayer at valley  $\nu$  respectively,  $\mathbb{T}$  is the tunneling interaction between the two interfacial layers,  $\mathbb{D} = \Delta \text{diag}(-2, -1, 0, 1, 2)_{\ell} \otimes \mathbb{1}_{\sigma}$  is the *external* interlayer displacement field that is diagonal in layer space  $\ell$  and is proportional to the identity matrix in sublattice space  $\sigma$ , and  $\nabla_{\mathbb{R}\pm\mathbf{r}}$  is a shorthand notation for rotating the gradient operator by  $\pm\theta/2$ . For accurate modeling, we include all known hoppings  $\{\gamma_0, \gamma_1, \gamma_2, \gamma_3, \gamma_4\} = \{-3.1, 0.38, -0.015, 0.29, 0.141\}$  eV [91–93] in  $\mathbb{K}_3$  and  $\mathbb{K}_2$  but we neglect the dimerization energy on eclipsed sites. In particular, the  $\gamma_3$  and  $\gamma_4$  terms that are responsible for trigonal warping can significantly deform the spectrum near charge neutrality. The tunneling matrix depends on two hopping parameters at the *AA* and *AB* regions of the twist interface  $\gamma_{AA}$  and  $\gamma_{AB}$ . Symmetry allows these two parameters to be different, and adjusting their relative amplitudes accounts for some lattice relaxation at the interface. Results in the main text are obtained using  $\gamma_{AA}/\gamma_{AB} = 0.1$  eV/0.12 eV [94–97]. In Ref. [98], we show that qualitative conclusions are robust against varying this ratio. That said, a comprehensive analysis of lattice relaxation is beyond the scope of the present work and is relegated to future studies.

TRMG<sub>3+2</sub> does not respect many point symmetries. Since rhombohedral multilayers of graphene do not respect  $C_{2z}$  symmetry, the twisted stack cannot either. Due to different layer numbers in the two substacks, symmetries that exchange layers across the twist interface like  $C_{2x}$  and  $C_{2y}$  rotations are automatically broken. However,  $C_{3z}$  symmetry is respected by each layer individually and hence is preserved in the twisted stack. Also, when both valleys are considered, time-reversal symmetry  $\mathcal{T}$  is respected. In our numerical calculations, we explicitly confirm that  $C_{3z}$  and  $\mathcal{T}$  symmetries are preserved in all cases.

At the non-interacting level, the band structure of TRMG<sub>3+2</sub> at zero displacement field for  $\theta \sim 1^\circ$  for both configurations features a pair of bands at charge neutrality per isospin flavor<sup>4</sup>. These bands are relatively narrow in spectral width (for instance, at  $\theta = 1.25^\circ$ , the bandwidth is about 25 meV), but they are *not* well isolated from the other higher energy bands. The suppressed bandwidth here mirrors the bandwidth of the active bands in twisted bilayer graphene, but in the latter scenario, the bands are also well isolated from the

rest of the band structure. Because of this spectral complexity, at zero displacement field, we heuristically do not expect that electron-electron interactions would isolate a single band with nontrivial topology. Indeed, extensive calculations that include Coulomb interactions confirm with this heuristic argument: the sought-after physics of a topologically nontrivial singlet band has to be found at non-zero displacement field.

The application of finite  $\Delta \neq 0$  has two qualitative effects on the band structure: (1) the shifting of the local spectra of the trilayer and bilayer subsystems relative to each other, and (2) the genesis of local gaps in each substack due to layer inequivalence (essentially, this is the effect of a  $\sigma_z$  mass). Interestingly, the formation of *local* gaps is *not* enough to generate a global gap in this system. To see this, let us consider the limit where the hoppings across the twist interface are switched off (i.e. the moiré structure can be gauged away) so that the subsystems can be regarded as independent. Placing the energy origin at the nodes of the multilayer spectra when  $\Delta = 0$ , the trilayer spectrum is centered at  $-\Delta$  with a gap of  $2|\Delta|$  and disperses away its extrema as  $\pm|\mathbf{k}|^3$ , while the bilayer spectrum is centered at  $3\Delta/2$  with a gap of  $|\Delta|$  and disperses away from its extrema as  $\pm|\mathbf{k}|^2$ . Importantly, for  $\Delta > 0$ , the conduction band minimum of the trilayer is located at  $E = 0$  while the valence band maximum of the bilayer is located at  $E = \Delta$ . Therefore, the two spectra completely overlap. For  $\Delta < 0$ , the valence band maximum of the trilayer is at  $E = 0$ , while the conduction band minimum of the bilayer is at  $E = \Delta$ . Thus, the same conclusion applies that the two independent spectra completely overlap. This simple analysis immediately traces the origin of any robust global gap in this system (which does indeed exist) to the existence of the moiré structure, elevating its important status in the subsequent analysis. For comparison, we recall that in rhombohedral graphene multilayers aligned with hBN, the role of the substrate in band-structure modeling is entirely negligible in the large  $\Delta$  limit where the conduction electrons are pushed to the layer farthest away from the substrate<sup>5</sup>; the giant gap at charge neutrality is just the gap of the graphene stack itself without any discernible contribution from the substrate [32, 33].

For  $\Delta < 0$ , the two active bands, initially entangled, are decoupled and pushed away from each other with increasing  $\Delta$ . Focusing on the conduction band, we find its states are predominantly localized on layer 1, suggesting that for negative  $\Delta$ , the trilayer plays a more dominant role than the bilayer. Not surprisingly then, we find that the conduction band can become very flat ( $< 5$  meV) because the  $\sqrt{\Delta^2 + |\mathbf{k}|^6}$  dispersion of the trilayer can be made narrow for reasonable values of  $\Delta$ . Now, band suppression does not always occur simultaneously with spectral isolation from the other bands. So, even though the conduction band can be made quite flat, it is often close by to, even if technically not overlapping, the next

<sup>4</sup> For the non-interacting band structures, valley-spin states are degenerate; so we shall restrict our discussion to just the  $\{\nu = +1, s = \uparrow\}$  flavor until interactions are considered where this degeneracy is broken.

<sup>5</sup> The role of the substrate on stabilizing the observed anomalous Hall effects is much more subtle and continues to generate debate and interest to the present [37, 99].

higher energy band. In contrast, when  $\Delta$  is increased in the positive direction, the conduction band is localized primarily on the bilayer sector. In this case, we seldom find bands as flat as in the negative  $\Delta$  direction. Of course, this is because the bilayer dispersion requires higher  $\Delta$  to flatten. As a result, all of the interesting correlated physics reported in this work is confined to the negative  $\Delta$  region of parameter space.

Spectrally, the band structures for both the antiparallel and parallel configurations are qualitatively similar. However, their differences are encoded in the quantum geometry of the Bloch states. For cases where the conduction band is fully gapped<sup>6</sup>, we calculate its Chern number and associated quantum metric violation defined as  $\lambda = (2\pi)^{-1} \int d^2\mathbf{k} [\text{Tr} g_{\mu\nu}(\mathbf{k}) - |\mathcal{B}_z(\mathbf{k})|]$ , where  $g_{\mu\nu}(\mathbf{k})$  is the quantum metric and  $\mathcal{B}_z(\mathbf{k})$  is the Berry curvature [100–104]. The  $\lambda$  quantity is a proxy for the propensity of a band to become an FCI once doped. It is based on analogy to the quantum geometry of the zeroth Landau level [78–80]. We shall use  $\lambda$  as a possible FCI diagnostic. The smaller it is, the better for FCIs. For comparison, the trace condition violations calculated for systems that have been experimentally shown to host FCI states are comparable to our values. For graphene pentalayer on hBN,  $\lambda \sim 0.6 - 1.45$  [32–34, 37]; for twisted MoTe<sub>2</sub>,  $\lambda \sim 0.1 - 0.7$  [22, 29, 105]. The Chern characterization of the antiparallel and parallel configurations in  $(\theta, \Delta)$  space is shown in Fig. 1(b,d). We find that the antiparallel configuration hosts a large region where  $\mathcal{C} = +2$ . In this region, the smallest trace condition violation is  $\lambda \approx 1.7$ . This coincides with the where the bandwidths are comparatively small ( $\sim 3$  meV) and band gaps relatively large  $\sim 6$  meV<sup>7</sup>. The parallel configuration is even more exotic in that it hosts both a  $\mathcal{C} = 2$  and a  $\mathcal{C} = 3$  region. The  $\mathcal{C} = 2$  region here features a slightly smaller trace condition violation, with  $\lambda \approx 1.3$  at best, compared to the antiparallel configuration. On the other hand, the  $\mathcal{C} = 3$  region has quite small  $\lambda < 1$ . However, the bandwidths of the  $\mathcal{C} = 3$  phase are generally larger ( $\sim 4.5$  meV) than the  $\mathcal{C} = 2$  phase ( $\sim 1.5$  meV). All in all, we find that for both the parallel and antiparallel configurations, there are regions with nonzero Chern numbers where relatively small bandwidths, large band gaps, and small  $\lambda$  coexist. We mark these regions with dashed lines in Fig. 1(b,d). From each region, we display a representative band structure in Fig. 1(c,e) showing the narrow band of interest polarized primarily to layer 1. We also show three band structures in Fig. 1(f,g,h) that seemingly do not look especially conducive to interaction effects, but yet they will turn out to be important once interactions are included.

A narrow band implies a large density of states, which, in

turn, suggests that electron-electron interactions should significantly modify these bands, both in terms of their energetic and topological properties. Therefore, the preceding analysis based on non-interacting band structures is only suggestive of a rough region in phase space where topologically nontrivial bands may give rise to higher-Chern anomalous quantum Hall phases. It is entirely possible that the inclusion of interactions may trivialize non-interacting Chern bands or topologicalize non-interacting trivial ones. As such, we need to account for Coulomb interactions in order to make reliable predictions. To this end, we perform self-consistent mean-field HF calculations. The mean-field Hamiltonian is written in band basis as

$$\hat{\mathcal{H}} = \sum_{\substack{\mathbf{k} \in \text{mBZ}, \\ n, n', \xi, \xi'}} \hat{\Psi}_{n, \xi, \mathbf{k}}^\dagger \left[ \mathbb{K}_{\xi, \xi', \mathbf{k}}^{n, n'} + \mathbb{H}_{\xi, \xi', \mathbf{k}}^{n, n'} + \mathbb{F}_{\xi, \xi', \mathbf{k}}^{n, n'} \right] \hat{\Psi}_{n', \xi', \mathbf{k}}, \quad (2)$$

where  $\hat{\Psi}_{n, \xi, \mathbf{k}}^\dagger$  is a fermionic creation operator for a Bloch state at momentum  $\mathbf{k}$ ,  $\{\xi, \xi', n, n'\}$  label isospins and bands respectively, and the kinetic energy (same as Eq. (1)), Hartree energy, and Fock exchange energy in the band basis are

$$\mathbb{K}_{\xi, \xi', \mathbf{k}}^{n, n'} = \delta_{\xi, \xi'} \delta_{n, n'} E_{n, \xi, \mathbf{k}}, \quad (3a)$$

$$\mathbb{H}_{\xi, \xi', \mathbf{k}}^{n, n'} = +\delta_{\xi, \xi'} \sum_{\substack{\mathbf{p} \in \text{mBZ} \\ n_1, n_3, \xi_1}} \mathbb{V}_{\xi_1, \xi, \mathbf{p}, \mathbf{k}, \mathbf{0}}^{n_1, n, n_3, n'} \mathbb{D}_{\xi_1, \xi_1, \mathbf{p}}^{n_1, n_3}, \quad (3b)$$

$$\mathbb{F}_{\xi, \xi', \mathbf{k}}^{n, n'} = - \sum_{\substack{\mathbf{p} \in \text{mBZ} \\ n_1, n_4}} \mathbb{V}_{\xi', \xi, \mathbf{k}, \mathbf{p}, \mathbf{p}-\mathbf{k}}^{n_1, n, n', n_4} \mathbb{D}_{\xi', \xi, \mathbf{p}}^{n_1, n_4}. \quad (3c)$$

In Eq. (3),  $E_{n, \xi, \mathbf{k}}$  are the non-interacting band eigenvalues, and the Coulomb matrix elements are calculated from layer-resolved form factors  $\mathbb{A}_{\xi, \ell, \mathbf{k}, \mathbf{q}+\mathbf{Q}}^{n, n'} = \langle u_{n, \xi, \mathbf{k}+\mathbf{q}} | e^{i\mathbf{Q} \cdot \hat{\mathbf{r}}} \mathbb{P}_\ell | u_{n', \xi, \mathbf{k}} \rangle$ , where  $\mathbb{P}_\ell$  is the projection to layer  $\ell$  and  $|u_{n, \xi, \mathbf{k}}\rangle$  are the periodic part of Bloch wavefunctions, as follows [106–108]

$$\mathbb{V}_{\xi_1, \xi_2, \mathbf{k}, \mathbf{p}, \mathbf{q}}^{n_1, n_2, n_3, n_4} = \sum_{\mathbf{Q}, \ell_1, \ell_2} \mathbb{A}_{\xi_1, \ell_1, \mathbf{k}, \mathbf{q}+\mathbf{Q}}^{n_1, n_3} \mathcal{V}_{\mathbf{q}+\mathbf{Q}}^{\ell_1, \ell_2} \mathbb{A}_{\xi_2, \ell_2, \mathbf{p}, -\mathbf{q}-\mathbf{Q}}^{n_2, n_4}, \quad (4a)$$

$$\mathcal{V}_{\mathbf{k}}^{\ell, \ell'} = \frac{e^2 \text{csch}(kD)}{2\epsilon_0 \epsilon_r k V_{\text{sys}}} [\cosh(k[D - |z_\ell - z_{\ell'}|]) - \cosh(k[D - |z_\ell + z_{\ell'}|])], \quad (4b)$$

where  $D$  is the distance between top and bottom gates,  $\epsilon_0$  and  $\epsilon_r$  are the permittivity of free space and dielectric constant respectively,  $V_{\text{sys}}$  is the system volume, and  $z_\ell$  is the vertical position of layer  $\ell$ . Throughout, lower-case momenta  $\mathbf{k}, \mathbf{p}, \mathbf{q}$  are confined within a moiré Brillouin zone (mBZ) while capitalized momenta  $\mathbf{Q}$  are reciprocal lattice vectors. We emphasize that we are using a layer-dependent Coulomb potential, Eq. (4b), that not only accounts for screening effects from the dual gates but also takes into consideration charge redistribution among the five layers to screen the applied displace-

<sup>6</sup> Fully gapped here means that it is gapped both above and below.

<sup>7</sup> There are also regions where  $|\mathcal{C}| = 1$ . Since we are interested in higher Chern numbers in this work, we do not analyze these regions here. However, it is perhaps worth mentioning that  $\lambda > 2$  for these regions. The bandwidth of the  $\mathcal{C} = -1$  region is relatively small ( $\sim 2.5$  meV), but the bandwidth of the  $\mathcal{C} = 1$  region is quite large ( $> 30$  meV).

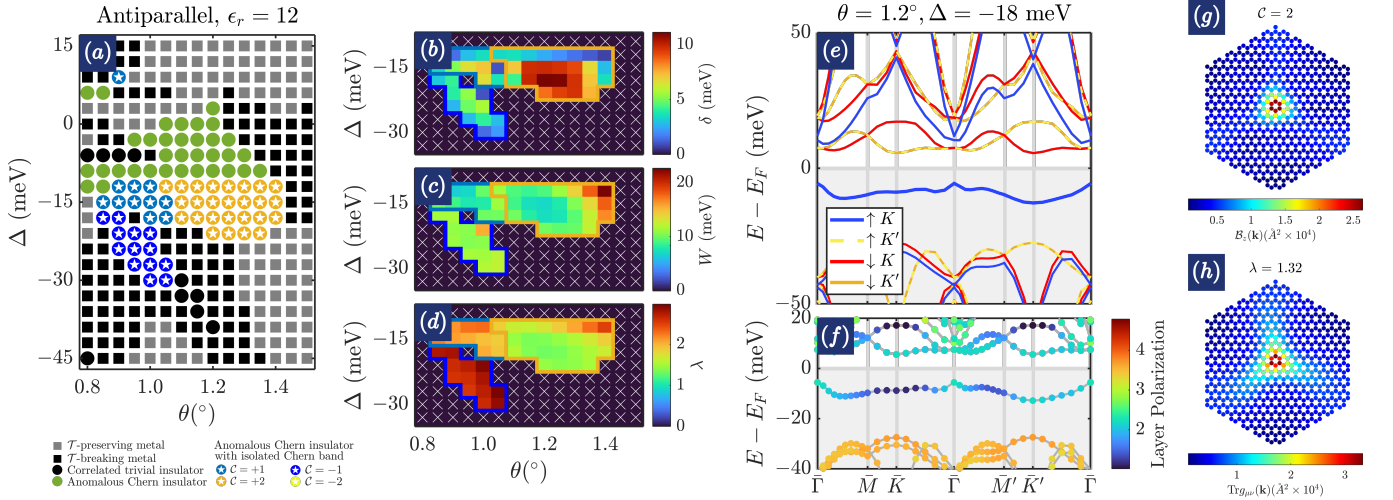


Figure 2. **Self-consistent mean field phase diagram of the antiparallel configuration and characterization of the  $\mathcal{C} = 2$  phase.** (a) Phase diagram in  $(\theta, \Delta)$  space showing several distinct metallic and insulating phases. Of particular interest is the presence of a  $\mathcal{C} = 2$  phase at negative  $\Delta$  and  $\theta \in [1.1^\circ, 1.4^\circ]$  featuring a spectrally-isolated, isospin-polarized, topologically-nontrivial band right below the Fermi level. The band gap, bandwidth, and trace condition violation of that band are shown in (b-d). A representative band structure from that phase color coded by isospin and by layer polarization is shown in (e) and (f) respectively. Here, the existence of an isolated narrow band with significant electron localization to the outermost layers of the trilayer substack is apparent. The distribution of the Berry curvature and quantum metric of that band in momentum space is plotted in (g) and (h) respectively. Here,  $\epsilon_r = 12$  and  $D = 40$  nm. Energies are measured relative to Fermi level,  $E_F$ .

ment field [107, 108]<sup>8</sup>. For simplicity, we assume that the graphene stack is located exactly half-way between the two gates. Unless specified otherwise,  $D = 40$  nm. In Eq. (3),  $\mathbb{D}_{\xi, \xi', \mathbf{p}}^{n, n'} = \langle \hat{\Psi}_{n, \xi, \mathbf{p}}^\dagger \hat{\Psi}_{n', \xi', \mathbf{p}} \rangle - \frac{1}{2} \delta_{n, n'} \delta_{\xi, \xi'}$  is the density matrix measured from a neutral uniform background at half filling in order to avoid double-counting Coulomb energy contributions already accounted for in *ab initio* calculations [109, 110].

In our iterative HF calculations, we only consider filling factor of one electron per moiré cell. Since we are only interested in valley-polarized anomalous quantum Hall phases, in analogy to the  $\text{MoTe}_2$  and the rhombohedral pentalayer system, we seed our calculations with initial ansatz that preferentially fill one of the isospin flavors with the extra electron per unit cell<sup>9</sup>. To determine the nature of the ground state, the energy of the converged solution from this symmetry-broken ansatz is compared to the solution of the corresponding symmetric state. As mentioned before, the gaps in the non-interacting model are not enormous (on the order of a few tens of meV at best, not hundreds) in the relevant regime of  $\Delta$ . Therefore, we need to include a decently large number of

bands in order to accurately capture Coulomb renormalization. In particular, there is no apparent sensible way to discard the valence bands as was customary in studies of pentalayer graphene on hBN [32–35, 40]. For the majority of the results in the main text, we include 8 (4 valence and 4 conduction) bands per isospin flavor. The grid size is always  $18 \times 18$  k points.

We first present the mean-field results for the antiparallel configuration in Fig. 2. We identify the following phases: (1) a  $\mathcal{T}$ -preserving metal resulting from the symmetric ansatz with total energy lower or very close to the solution of the symmetry-broken ansatz, (2) a  $\mathcal{T}$ -breaking metal that unequally occupies the isospin flavors and contains a Fermi surface, (3) a correlated trivial insulator that breaks  $\mathcal{T}$ -symmetry and is gapped phase with zero Hall conductivity, (4) an anomalous Chern insulator that features quantized Hall conductivity but *without* an isolated Chern band right below chemical potential, and (5) an anomalous Chern insulator with isolated Chern band and quantized Hall conductivity whose first valence band is spectrally-isolated, topological band. The last phase is what we are after in this work since its existence suggests the possibility of exotic fractionalized states upon partial doping. We label this state by the Chern number of its first valence band (which is often, but not always, the same as the Hall conductivity of the corresponding gap at Fermi level), which we will use to refer to this state henceforth. The phase diagram simulated with  $\epsilon_r = 12$  is shown in Fig. 2(a). As is evident, the phase diagram features considerable complexity owing to the complex evolution of the band structure as a function of  $\theta$  and  $\Delta$ . All five phases aforementioned are

<sup>8</sup> The simple form of the Coulomb potential assumes that the bottom gate is located at  $z = 0$  and the top gate is located at  $z = D$ . We provide the full derivation of this Coulomb potential using Green's functions in Ref. [98]. There, we also compare this functional form of the Coulomb potential at  $\mathbf{k} = \mathbf{0}$  to the classical capacitor model and find exact agreement (see also Refs. [107, 108]). As a quick consistency check here, if we take  $z_\ell = z_{\ell'} = D/2$ , we obtain exactly the usual dual-gate potential:  $\mathcal{V}_{\mathbf{k}} = e^2 \tanh(kD/2) / 2\epsilon_0 \epsilon_r k V_{\text{sys}}$ .

<sup>9</sup> Searching for more general ground states such as valley-coherent states or nematic states would form an interesting further study.

represented in this phase diagram. Most importantly, we find the  $C = 2$  phase spanning an angle range  $\theta \in [1.1^\circ, 1.4^\circ]$  for  $\Delta \in [-21, -12]$  meV. We also find a region where  $|C| = 1$  at smaller angles.

Focusing on the  $C = 2$  phase, we further characterize its spectral and quantum geometric properties in Fig. 1(b-d). We quantify an “optimal” combination of  $(\theta, \Delta)$  within this phase with a figure of merit defined simply as f.o.m. =  $\delta/W\lambda$ , where  $\delta$  is the minimum of the gaps above and below the band of interest and  $W$  is its bandwidth. A large f.o.m. means that the band is susceptible to further renormalization by residual Coulomb interactions once partially doped and that the band has a small trace condition violation. In other words, this band is a candidate for hosting a fractional quantum hall phase that requires strong Coulomb repulsion to stabilize. A similar, but not the same, f.o.m. is used in Ref. [33, 111]. For the  $C = 2$  phase, the optimal f.o.m. occurs at  $\theta = 1.20^\circ$  and  $\Delta = -18$  meV where  $W = 7.5$  meV,  $\delta = 11.1$  meV,  $\lambda = 1.32$ . Referring back to the non-interacting band structures in Fig. 1(f), we find that the band is not even fully gapped without interactions at this  $(\theta, \Delta)$ . Therefore, we attribute the origins of this isolated topological band to Coulomb interactions. The HF-renormalized bands color coded by isospin polarization and valley polarization are shown in Fig. 2(e) and (f) respectively. The Berry curvature and quantum metric of this band, shown in Fig. 2(g,h), are concentrated primarily at the  $\Gamma$  point. Remarkably, we find that interactions reduce the optimal values of  $\lambda$ ,  $\lambda = 1.7 \rightarrow 1.32$ . As is clear from Fig. 2(f), the electrons in this band are localized mostly in layer 1, validating a prior assertion that the trilayer substack plays the dominant role in the observed physics. Once the charge density is summed over all states from that band, we find that the total charge density has  $\gtrsim 70\%$  of its share on layer 1, where the charge density also fluctuates laterally with a higher concentration at one of the three Wyckoff positions in the moiré unit cell.

Next, we present the mean-field results for the parallel configuration in Fig. 3. We again find in Fig. 3(a) a plethora of metallic and insulating phases. Crucially, we find a prominent contiguous region that starts with  $C = 2$  at lower angles and crosses over to  $C = 3$  at larger angles. Again, while these phases no doubt are related to the  $C = 2$  and  $C = 3$  bands in the non-interacting limit, we emphasize that they occur here in the HF phase diagram at values of  $(\theta, \Delta)$  where the non-interacting band structures do not feature a fully isolated Chern band near charge neutrality. Thus, comparing to Fig. 1(g,h) in the non-interacting limit, these fully-isolated bands must be stabilized by Coulomb interactions. For the  $C = 2$  phase, optimal f.o.m. occurs at  $\theta = 1.1^\circ$  and  $\Delta = -21$  meV where  $\delta = 7.9$  meV,  $W = 3.8$  meV, and  $\lambda = 0.87$ . The band structure at this value of  $(\theta, \Delta)$  is shown in Fig. 3(e,f). We notice that the band is exceptionally narrow with a smaller gap above and a much larger gap below. The Berry curvature is more delocalized in this case, as shown in Fig. 3(g), compared to the antiparallel situation. As before, we find that Coulomb interactions reduce  $\lambda$ . After HF renormalization, optimal  $\lambda \approx 0.9$  is smaller than the non-interacting

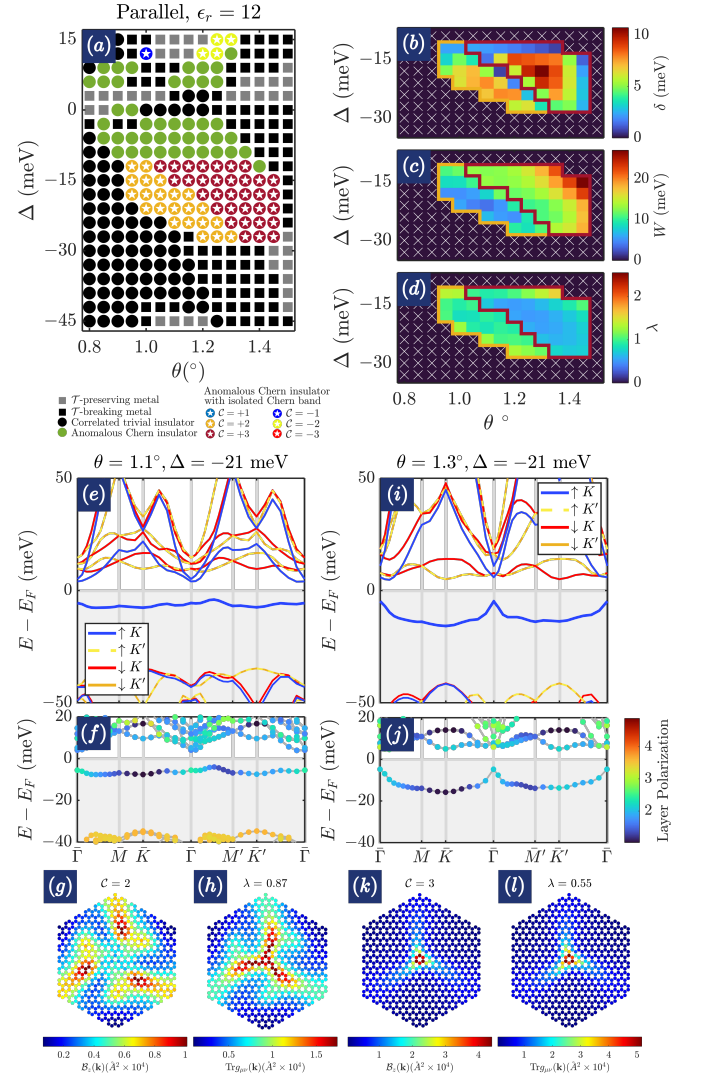


**Figure 3. Self-consistent mean field phase diagram of the parallel configuration and characterization of the  $C = 2$  and  $C = 3$  phases.** (a) Phase diagram in  $(\theta, \Delta)$  space showing several distinct metallic and insulating phases. Of importance is the presence of a contiguous region showing  $C = 2$  and  $C = 3$  phases at negative  $\Delta$  and  $\theta \in [0.95^\circ, 1.45^\circ]$  featuring a spectrally-isolated, isospin-polarized, topologically-nontrivial bands right below the Fermi level. The band gap, bandwidth, and trace condition violation of that band are shown in (b-d). A representative band structure for the  $C = 2$  phase color coded by isospin and by layer polarization is shown in (e) and (f) respectively. The band of interest is exceptionally narrow with large gap below and a smaller gap above. A representative band structure for the  $C = 3$  phase color coded by isospin and by layer polarization is shown in (i) and (j) respectively. The bandwidth of this phase is not as small as the  $C = 2$  phase. The distribution of the Berry curvature and quantum metric is shown in (g,h,k,l). Here,  $\epsilon_r = 12$  and  $D = 40$  nm. Energies are measured relative to Fermi level,  $E_F$ .

values around  $\lambda \approx 1.3$ . Moving onto the  $C = 3$  phase, we find that optimal f.o.m. occurs at a higher angle  $\theta = 1.3^\circ$  but same  $\Delta = -21$  meV. Here,  $\delta = 9.5$  meV while  $W = 11$  meV. Generally, we find that the  $C = 3$  phase features large

bandwidths compared to the  $\mathcal{C} = 2$  phases both in the parallel and antiparallel configurations. This is perhaps a bit surprising considering the energy spectra for both Chern phases are similar in the non-interacting limit, highlighting the role of wavefunctions (form factors) in controlling the interaction renormalization of electronic properties. The trace condition violation here is remarkably low  $\lambda = 0.55$ ; it is already low in the non-interacting limit,  $\lambda \approx 0.75$ , but HF renormalization reduces it even more. Thus, we find in all cases that Coulomb interactions have the tendency to lower the trace condition violation<sup>10</sup>. The Berry curvature and quantum metric for the  $\mathcal{C} = 3$  phase are both concentrated at the  $\bar{\Gamma}$  point, as shown in Fig. 3(k,l). The charge densities for both the  $\mathcal{C} = 2$  and  $\mathcal{C} = 3$  phases are localized primarily on layer 1 ( $\gtrsim 75\%$ ). On that layer, the charge density fluctuates laterally as well, with more concentration at one of the three Wyckoff positions in the moiré unit cell. However, the  $\mathcal{C} = 2$  phase chooses a different Wyckoff position to localize charge compared to the  $\mathcal{C} = 3$  phase.

In both stacking configurations, we have established that electron-electron interactions at  $\epsilon_r = 12$  and  $D = 40$  nm are favorable to the formation of topologically-nontrivial bands that give rise to anomalous quantum Hall phases at an integer filling and are possible candidates for fractional quantum Hall phases at partial fillings. Coulomb interactions generate fully-isolated, relatively-narrow bands for values of  $(\theta, \Delta)$  where these bands are entangled with other bands in the non-interacting limit; Coulomb interactions also reduce the quantum metric violation in these phases compared to their non-interacting counterparts. From the presented phase diagrams, it is also clear that these phases are robust with variations in  $\Delta$  and  $\theta$  because the phase regions span prominent domains in phase space. In other words, no fine tuning of  $\theta$  or  $\Delta$  is necessary.

Next, we analyze the stability of these phases as the Coulomb interaction is modified. This is an important consideration because the strength of electron-electron interactions can be experimentally controlled by dielectric engineering (changing  $\epsilon_r$ ) and gate distance (changing  $D$ ). For this purpose, we park ourselves at a particular  $(\theta, \Delta)$  and sweep  $(D, \epsilon_r)$ . For demonstration, we choose the optimal combinations of  $(\theta, \Delta)$  as diagnosed by f.o.m. in the preceding analysis. The results are shown in Fig. 4. In general, all of these states seem quite insensitive to changing the gate distance  $D$ . The dependence on  $\epsilon_r$  is more intricate. In Fig. 4(a), we assess the stability of the antiparallel configuration for a  $\mathcal{C} = 2$  state. As is clear, this state is robust for  $\epsilon_r < 21$ . At the high-

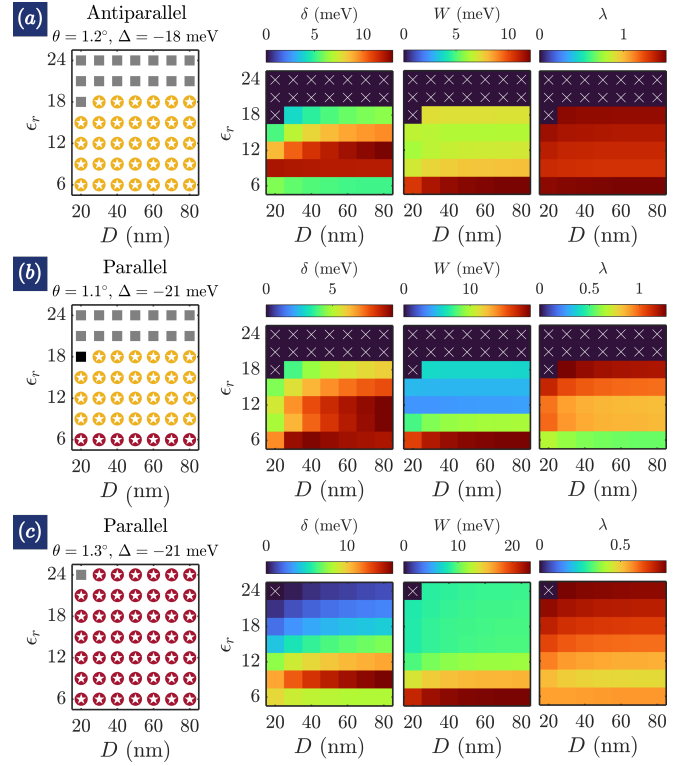


Figure 4. **Stability of topologically nontrivial phases.** We show the evolution of states at fixed  $(\theta, \Delta)$  as a function of  $(D, \epsilon_r)$ . In the first column, we classify the states using the same method as in Figs. 2 and 3. In the second to fourth columns, we characterize the band gap, bandwidth, and trace condition violation of the band of interest for values of  $(D, \epsilon_r)$  where it is isolated. For these simulations, we include 6 bands per isospin.

est  $\epsilon_r > 21$  (i.e. the weakest Coulomb strength), this state is out-competed by the symmetric metallic state. The value of  $\epsilon_r \sim 9 - 15$  appears optimal for this state and lies in the range of  $\epsilon_r$  that are typically used to .  $\lambda$  remains relatively unchanged as  $\epsilon_r$  and  $D$  are varied. For a  $\mathcal{C} = 2$  state in the parallel configuration, we again observe that there is a finite range of  $\epsilon_r \sim 9 - 18$  where this phase exists. For weaker Coulomb interactions (larger  $\epsilon_r$ ), this state is outcompeted by the symmetric metallic phase too. For smaller  $\epsilon_r \sim 6$ , this state merges into a  $\mathcal{C} = 3$  state. The  $\mathcal{C} = 3$  state in the parallel configuration is much more robust than the other two states. It persists essentially in the entire domain of  $(D, \epsilon_r)$  for our scan. The optimal dielectric constant occurs around  $\epsilon_r = 9$ . We also show extensive phase diagrams for  $\epsilon_r \sim 6$  in Ref. [98].

In Ref. [98], we consider many other different perturbations to assess the robustness of our predictions. In particular, we study the absence of lattice relaxation, i.e.  $\gamma_{AA}/\gamma_{AB} = 1$ , the role of reduced  $\gamma_0 = 2.7$  eV<sup>11</sup> [112, 113], and the neglect of layer dependence on the Coulomb potential energy,

<sup>10</sup> By this, we mean that in both configurations and for both  $\mathcal{C} = 2$  and  $\mathcal{C} = 3$ , the optimal values of  $\lambda$  are reduced after including HF interactions. We note, however, that the optimal values of  $\lambda$  may occur at different points in  $(\theta, \Delta)$  space. We have not done a systematic comparison of  $\lambda$  before and after HF renormalization for the same values of  $(\theta, \Delta)$  because it is not always sensible to do so since there are many instances where the non-interacting bands are not gapped but the HF bands are gapped and vice versa.

<sup>11</sup> It appears that there is no consensus on the value of  $\gamma_0$  in the literature.

i.e.  $\mathcal{V}_k \propto \tanh(kD/2)/k$ . We find that the  $\mathcal{C} = 2$  phase in the antiparallel configuration is robust in all the cases examined. The parallel configuration is more sensitive to changes in parameters. While both Chern  $\mathcal{C} = 2$  and  $\mathcal{C} = 3$  phases always exist, we find that their areas in phase space can be significantly enlarged or diminished depending on simulation parameters. Nevertheless, we emphasize again that we always find that either  $\mathcal{C} = 2$ ,  $\mathcal{C} = 3$ , or both phases exist. We provide further discussion of the robustness of these phases in Ref. [98].

We end by addressing a question that naturally follows the preceding discussion: to which of the two known experimental FCI systems is our platform similar? The quick answer is that our system shares similarities with both, but also exhibits some distinct properties. Here, we set aside the obvious difference that our system features  $|\mathcal{C}| > 1$  unlike the two experimental systems that have  $|\mathcal{C}| = 1$ . On one hand, the isolated nontrivial bands already exist in the non-interacting limit, like in twisted  $\text{MoTe}_2$ . On the other, optimal values of  $(\theta, \Delta)$  where isolated bands with favorable quantum geometry exist after HF renormalization are where non-interacting bands are not isolated at all, like in graphene-hBN heterostructures. Furthermore, a majority of the electron population for the active band resides on the outer layer of the trilayer substack, bearing resemblance to the electronic occupation in the conduction band of graphene-hBN heterostructures under a displacement field. However, the role of the moiré structure (e.g. the twist interface) is important in our system as it would not be gapped otherwise even with a displacement field, unlike in graphene-hBN heterostructures where the large gap below the flat band is field-induced<sup>12</sup>. Therefore, from our perspective, it is fairest to say that our system is a paradigm of its own, with important similarities and differences to both of the known FCI systems.

In this work, we have demonstrated that  $\text{TRMG}_{3+2}$  is likely an anomalous Chern insulator whose valence bands immediately below the Fermi level have  $|\mathcal{C}| > 1$ . These phases are stabilized by Coulomb interactions. Most interestingly, the isolated, narrow, HF-renormalized bands only mildly violate the trace condition. Therefore, we are optimistic that our proposed platform might also become an FCI

once partially doped. In the present work, we have not explored the different possible FCI states that can form in this system [49–55]. In the near future, we shall report results from ongoing work devoted to exploring such possibilities using numerical techniques suitable for calculating strongly-correlated ground states (such as many-body exact diagonalization).  $\text{TRMG}_{3+2}$  is just one example in a family of twisted materials constructed from an  $M$ -layer rhombohedral stack rotationally misaligned on top of an  $N$ -layer rhombohedral stack,  $\text{TRMG}_{M+N}$ . We expect these related systems to contain similar phases, perhaps even with higher Chern numbers for isolated narrow bands. Our hypothesis is supported by the fact that all of the relevant high-Chern phases in  $\text{TRMG}_{3+2}$  occur in regions of displacement field where the electron occupation is peaked on the trilayer substack (rather than the bilayer substack), suggesting that higher layer number associated with flat-band formation may have an outsized influence on the observed phenomenology. Our results demonstrate that layer number adds yet another ingredient to an already-versatile set of tunable knobs (relative stacking order, displacement field, twist angle, etc...) endowed to this family of materials. Therefore, we expect continued investigation into  $\text{TRMG}_{M+N}$  to yield a rich understanding of correlated and fractionalized physics.

We thank Eugene J. Mele, Francisco Guinea, Nicholas Bonesteel, Mitali Banerjee, Matthew Yankowitz, and Xirui Wang for fruitful discussions. We are grateful to Hitesh Changlani for sharing computational resources. Numerical calculations are done using the High Performance Compute Cluster of the Research Computing Center (RCC) at Florida State University. This work was supported by start-up funds from Florida State University and the National High Magnetic Field Laboratory and also by an intramural award from the Florida State University's Provost's Office and the Office of Postdoctoral Affairs. The National High Magnetic Field Laboratory is supported by the National Science Foundation through NSF/DMR-2128556 and the State of Florida.

---

Values extracted from experiments tend to be at the higher end 3.1 – 3.2 eV [91–93], while values calculated from density functional theory tend to be at the lower end 2.6 – 2.7 eV [112, 113]. We take the perspective that experimentally-extracted values are more representative of reality. In the interest of making realistic predictions, all results presented in the main text are simulated with a higher value of  $\gamma_0$ . However, to their assess robustness, we also show results simulated with a smaller  $\gamma_0$  in Ref. [98].

<sup>12</sup> An interesting investigation for future work might be to carefully explore if electron-electron interactions alone would be enough to generate the isolated narrow Chern bands even when one completely turns off the hoppings across the twist interface. That is, when the moiré structure is non-existent, what happens to the correlated phases? However the answer to this interesting question turns out to be, it shall have no material effect on the conclusions of the present work. The fact that we observe qualitatively different phase diagrams depending on alignment configuration already points to the importance of the twist interface in our system.

\* vophong@magnet.fsu.edu

† clewandowski@magnet.fsu.edu

- [1] T. Neupert, L. Santos, C. Chamon, and C. Mudry, Fractional quantum hall states at zero magnetic field, *Phys. Rev. Lett.* **106**, 236804 (2011).
- [2] E. Tang, J.-W. Mei, and X.-G. Wen, High-temperature fractional quantum hall states, *Phys. Rev. Lett.* **106**, 236802 (2011).
- [3] K. Sun, Z. Gu, H. Katsura, and S. Das Sarma, Nearly flatbands with nontrivial topology, *Phys. Rev. Lett.* **106**, 236803 (2011).
- [4] N. Regnault and B. A. Bernevig, Fractional chern insulator, *Phys. Rev. X* **1**, 021014 (2011).
- [5] Y.-L. Wu, B. A. Bernevig, and N. Regnault, Zoology of fractional chern insulators, *Phys. Rev. B* **85**, 075116 (2012).
- [6] S. A. Parameswaran, R. Roy, and S. L. Sondhi, Fractional chern insulators and the  $W_\infty$  algebra, *Phys. Rev. B* **85**, 241308 (2012).

- [7] J. Behrmann, Z. Liu, and E. J. Bergholtz, Model fractional chern insulators, *Phys. Rev. Lett.* **116**, 216802 (2016).
- [8] M. Greiter and F. Wilczek, Fractional statistics, *Annu. Rev. Condens. Matter Phys.* **15**, 131 (2024).
- [9] C. Nayak, S. H. Simon, A. Stern, M. Freedman, and S. Das Sarma, Non-abelian anyons and topological quantum computation, *Rev. Mod. Phys.* **80**, 1083 (2008).
- [10] J. Cai, E. Anderson, C. Wang, X. Zhang, X. Liu, W. Holtzmann, Y. Zhang, F. Fan, T. Taniguchi, K. Watanabe, *et al.*, Signatures of fractional quantum anomalous hall states in twisted mote2, *Nature* **622**, 63 (2023).
- [11] Y. Zeng, Z. Xia, K. Kang, J. Zhu, P. Knüppel, C. Vaswani, K. Watanabe, T. Taniguchi, K. F. Mak, and J. Shan, Thermodynamic evidence of fractional chern insulator in moiré mote2, *Nature* **622**, 69 (2023).
- [12] F. Xu, Z. Sun, T. Jia, C. Liu, C. Xu, C. Li, Y. Gu, K. Watanabe, T. Taniguchi, B. Tong, J. Jia, Z. Shi, S. Jiang, Y. Zhang, X. Liu, and T. Li, Observation of integer and fractional quantum anomalous hall effects in twisted bilayer mote2, *Phys. Rev. X* **13**, 031037 (2023).
- [13] E. Redekop, C. Zhang, H. Park, J. Cai, E. Anderson, O. Sheekey, T. Arp, G. Babikyan, S. Salters, K. Watanabe, *et al.*, Direct magnetic imaging of fractional chern insulators in twisted mote2, *Nature* **635**, 584 (2024).
- [14] Z. Ji, H. Park, M. E. Barber, C. Hu, K. Watanabe, T. Taniguchi, J.-H. Chu, X. Xu, and Z.-X. Shen, Local probe of bulk and edge states in a fractional chern insulator, *Nature* **635**, 578 (2024).
- [15] F. Xu, Z. Sun, J. Li, C. Zheng, C. Xu, J. Gao, T. Jia, K. Watanabe, T. Taniguchi, B. Tong, *et al.*, Signatures of unconventional superconductivity near reentrant and fractional quantum anomalous hall insulators, arXiv preprint arXiv:2504.06972 <https://doi.org/10.48550/arXiv.2504.06972> (2025).
- [16] H. Park, W. Li, C. Hu, C. Beach, M. Gonçalves, J. F. Mendez-Valderrama, J. Herzog-Arbeitman, T. Taniguchi, K. Watanabe, D. Cobden, *et al.*, Observation of high-temperature dissipationless fractional chern insulator, arXiv preprint arXiv:2503.10989 <https://doi.org/10.48550/arXiv.2503.10989> (2025).
- [17] Y. Wang, J. Choe, E. Anderson, W. Li, J. Ingham, E. A. Arsenault, Y. Li, X. Hu, T. Taniguchi, K. Watanabe, *et al.*, Hidden states and dynamics of fractional fillings in tmote2 moiré superlattices, arXiv preprint arXiv:2502.21153 <https://doi.org/10.48550/arXiv.2502.21153> (2025).
- [18] X. Chang, F. Liu, F. Xu, C. Xu, J. Xiao, Z. Sun, P. Jiao, Y. Zhang, S. Wang, B. Shen, *et al.*, Emergent charge-transfer ferromagnetism and fractional chern states in moiré mote2, arXiv preprint arXiv:2503.13213 <https://doi.org/10.48550/arXiv.2503.13213> (2025).
- [19] Z. Lu, T. Han, Y. Yao, A. P. Reddy, J. Yang, J. Seo, K. Watanabe, T. Taniguchi, L. Fu, and L. Ju, Fractional quantum anomalous hall effect in multilayer graphene, *Nature* **626**, 759 (2024).
- [20] J. Xie, Z. Huo, X. Lu, Z. Feng, Z. Zhang, W. Wang, Q. Yang, K. Watanabe, T. Taniguchi, K. Liu, *et al.*, Tunable fractional chern insulators in rhombohedral graphene superlattices, *Nature Materials*, 1 (2025).
- [21] Z. Lu, T. Han, Y. Yao, Z. Hadjri, J. Yang, J. Seo, L. Shi, S. Ye, K. Watanabe, T. Taniguchi, *et al.*, Extended quantum anomalous hall states in graphene/hbn moiré superlattices, *Nature*, 1 (2025).
- [22] A. P. Reddy and L. Fu, Toward a global phase diagram of the fractional quantum anomalous hall effect, *Phys. Rev. B* **108**, 245159 (2023).
- [23] A. P. Reddy, F. Alsallom, Y. Zhang, T. Devakul, and L. Fu, Fractional quantum anomalous hall states in twisted bilayer mote2 and wse2, *Phys. Rev. B* **108**, 085117 (2023).
- [24] C. Wang, X.-W. Zhang, X. Liu, Y. He, X. Xu, Y. Ran, T. Cao, and D. Xiao, Fractional chern insulator in twisted bilayer mote2, *Phys. Rev. Lett.* **132**, 036501 (2024).
- [25] N. Morales-Durán, N. Wei, J. Shi, and A. H. MacDonald, Magic angles and fractional chern insulators in twisted homobilayer transition metal dichalcogenides, *Phys. Rev. Lett.* **132**, 096602 (2024).
- [26] J. Shi, N. Morales-Durán, E. Khalaf, and A. H. MacDonald, Adiabatic approximation and aharonov-casher bands in twisted homobilayer transition metal dichalcogenides, *Phys. Rev. B* **110**, 035130 (2024).
- [27] Y. Jia, J. Yu, J. Liu, J. Herzog-Arbeitman, Z. Qi, H. Pi, N. Regnault, H. Weng, B. A. Bernevig, and Q. Wu, Moiré fractional chern insulators. i. first-principles calculations and continuum models of twisted bilayer mote2, *Phys. Rev. B* **109**, 205121 (2024).
- [28] J. Yu, J. Herzog-Arbeitman, M. Wang, O. Vafek, B. A. Bernevig, and N. Regnault, Fractional chern insulators versus nonmagnetic states in twisted bilayer mote2, *Phys. Rev. B* **109**, 045147 (2024).
- [29] C. Xu, J. Li, Y. Xu, Z. Bi, and Y. Zhang, Maximally localized wannier functions, interaction models, and fractional quantum anomalous hall effect in twisted bilayer mote2, *Proc. Natl. Acad. Sci. U.S.A.* **121**, e2316749121 (2024).
- [30] B. Li and F. Wu, Variational mapping of chern bands to landau levels: Application to fractional chern insulators in twisted mote2, *Phys. Rev. B* **111**, 125122 (2025).
- [31] J. Chen, Q. Li, X. Wang, and W. Li, Fractional chern insulator and quantum anomalous hall crystal in twisted mote2, arXiv preprint arXiv:2504.07932 <https://doi.org/10.48550/arXiv.2504.07932> (2025).
- [32] J. Dong, T. Wang, T. Wang, T. Soejima, M. P. Zaletel, A. Vishwanath, and D. E. Parker, Anomalous hall crystals in rhombohedral multilayer graphene. i. interaction-driven chern bands and fractional quantum hall states at zero magnetic field, *Phys. Rev. Lett.* **133**, 206503 (2024).
- [33] B. Zhou, H. Yang, and Y.-H. Zhang, Fractional quantum anomalous hall effect in rhombohedral multilayer graphene in the moiréless limit, *Phys. Rev. Lett.* **133**, 206504 (2024).
- [34] Z. Dong, A. S. Patri, and T. Senthil, Theory of quantum anomalous hall phases in pentalayer rhombohedral graphene moiré structures, *Phys. Rev. Lett.* **133**, 206502 (2024).
- [35] Z. Dong, A. S. Patri, and T. Senthil, Stability of anomalous hall crystals in multilayer rhombohedral graphene, *Phys. Rev. B* **110**, 205130 (2024).
- [36] Y. H. Kwan, J. Yu, J. Herzog-Arbeitman, D. K. Efetov, N. Regnault, and B. A. Bernevig, Moiré fractional chern insulators iii: Hartree-fock phase diagram, magic angle regime for chern insulator states, the role of the moiré potential and goldstone gaps in rhombohedral graphene superlattices, arXiv preprint arXiv:2312.11617 <https://doi.org/10.48550/arXiv.2312.11617> (2023).
- [37] J. Herzog-Arbeitman, Y. Wang, J. Liu, P. M. Tam, Z. Qi, Y. Jia, D. K. Efetov, O. Vafek, N. Regnault, H. Weng, Q. Wu, B. A. Bernevig, and J. Yu, Moiré fractional chern insulators. ii. first-principles calculations and continuum models of rhombohedral graphene superlattices, *Phys. Rev. B* **109**, 205122 (2024).
- [38] Z. Guo, X. Lu, B. Xie, and J. Liu, Fractional chern insulator states in multilayer graphene moiré superlattices, *Phys. Rev. B* **110**, 075109 (2024).

- [39] K. Huang, X. Li, S. Das Sarma, and F. Zhang, Self-consistent theory of fractional quantum anomalous hall states in rhombohedral graphene, *Phys. Rev. B* **110**, 115146 (2024).
- [40] T. Soejima, J. Dong, T. Wang, T. Wang, M. P. Zaletel, A. Vishwanath, and D. E. Parker, Anomalous hall crystals in rhombohedral multilayer graphene. ii. general mechanism and a minimal model, *Phys. Rev. B* **110**, 205124 (2024).
- [41] K. Huang, S. Das Sarma, and X. Li, Fractional quantum anomalous hall effect in rhombohedral multilayer graphene with a strong displacement field, *Phys. Rev. B* **111**, 075130 (2025).
- [42] T. Tan and T. Devakul, Parent berry curvature and the ideal anomalous hall crystal, *Phys. Rev. X* **14**, 041040 (2024).
- [43] H. Li, B. A. Bernevig, and N. Regnault, Multi-band exact diagonalization and an iteration approach to hunt for fractional chern insulators in rhombohedral multilayer graphene, *arXiv preprint arXiv:2504.20140* <https://doi.org/10.48550/arXiv.2504.20140> (2025).
- [44] H. Min and A. H. MacDonald, Chiral decomposition in the electronic structure of graphene multilayers, *Phys. Rev. B* **77**, 155416 (2008).
- [45] M. Koshino and E. McCann, Trigonal warping and berry's phase  $n\pi$  in abc-stacked multilayer graphene, *Phys. Rev. B* **80**, 165409 (2009).
- [46] F. Zhang, B. Sahu, H. Min, and A. H. MacDonald, Band structure of *abc*-stacked graphene trilayers, *Phys. Rev. B* **82**, 035409 (2010).
- [47] M. Z. Hasan and C. L. Kane, Colloquium: Topological insulators, *Rev. Mod. Phys.* **82**, 3045 (2010).
- [48] X.-L. Qi and S.-C. Zhang, Topological insulators and superconductors, *Rev. Mod. Phys.* **83**, 1057 (2011).
- [49] Y.-F. Wang, H. Yao, C.-D. Gong, and D. N. Sheng, Fractional quantum hall effect in topological flat bands with chern number two, *Phys. Rev. B* **86**, 201101 (2012).
- [50] M. Barkeshli and X.-L. Qi, Topological nematic states and non-abelian lattice dislocations, *Phys. Rev. X* **2**, 031013 (2012).
- [51] Z. Liu, E. J. Bergholtz, H. Fan, and A. M. Läuchli, Fractional chern insulators in topological flat bands with higher chern number, *Phys. Rev. Lett.* **109**, 186805 (2012).
- [52] A. Sterdyniak, C. Repellin, B. A. Bernevig, and N. Regnault, Series of abelian and non-abelian states in  $c > 1$  fractional chern insulators, *Phys. Rev. B* **87**, 205137 (2013).
- [53] T. Liu, C. Repellin, B. A. Bernevig, and N. Regnault, Fractional chern insulators beyond Laughlin states, *Phys. Rev. B* **87**, 205136 (2013).
- [54] G. Möller and N. R. Cooper, Fractional chern insulators in harper-hofstadter bands with higher chern number, *Phys. Rev. Lett.* **115**, 126401 (2015).
- [55] B. Andrews, T. Neupert, and G. Möller, Stability, phase transitions, and numerical breakdown of fractional chern insulators in higher chern bands of the hofstadter model, *Phys. Rev. B* **104**, 125107 (2021).
- [56] N. R. Chebrolu, B. L. Chittari, and J. Jung, Flat bands in twisted double bilayer graphene, *Phys. Rev. B* **99**, 235417 (2019).
- [57] M. Koshino, Band structure and topological properties of twisted double bilayer graphene, *Phys. Rev. B* **99**, 235406 (2019).
- [58] Z. Liu, A. Abouelkomsan, and E. J. Bergholtz, Gate-tunable fractional chern insulators in twisted double bilayer graphene, *Phys. Rev. Lett.* **126**, 026801 (2021).
- [59] R. Perea-Causin, H. Liu, and E. J. Bergholtz, Quantum anomalous hall crystals in moiré bands with higher chern number, *arXiv preprint arXiv:2412.02745* <https://doi.org/10.48550/arXiv.2412.02745> (2024).
- [60] Y.-H. Zhang, D. Mao, Y. Cao, P. Jarillo-Herrero, and T. Senthil, Nearly flat chern bands in moiré superlattices, *Phys. Rev. B* **99**, 075127 (2019).
- [61] T. Devakul, P. J. Ledwith, L.-Q. Xia, A. Uri, S. C. de la Barrera, P. Jarillo-Herrero, and L. Fu, Magic-angle helical trilayer graphene, *Sci. Adv.* **9**, eadi6063 (2023).
- [62] Y. H. Kwan, P. J. Ledwith, C. F. B. Lo, and T. Devakul, Strong-coupling topological states and phase transitions in helical trilayer graphene, *Phys. Rev. B* **109**, 125141 (2024).
- [63] A. Datta, D. Guerci, M. O. Goerbig, and C. Mora, Helical trilayer graphene in magnetic field: Chern mosaic and higher chern number ideal flat bands, *Phys. Rev. B* **110**, 075417 (2024).
- [64] R. Makov, F. Guinea, and A. Stern, Flat bands in chiral multilayer graphene, *Phys. Rev. B* **110**, 195112 (2024).
- [65] X. Wan, S. Sarkar, K. Sun, and S.-Z. Lin, Nearly flat chern band in periodically strained monolayer and bilayer graphene, *Phys. Rev. B* **108**, 125129 (2023).
- [66] M. Fujimoto, D. E. Parker, J. Dong, E. Khalaf, A. Vishwanath, and P. Ledwith, Higher vortexability: Zero-field realization of higher Landau levels, *Phys. Rev. Lett.* **134**, 106502 (2025).
- [67] S. A. A. Ghorashi, A. Dunbrack, A. Abouelkomsan, J. Sun, X. Du, and J. Cano, Topological and stacked flat bands in bilayer graphene with a superlattice potential, *Phys. Rev. Lett.* **130**, 196201 (2023).
- [68] S. A. A. Ghorashi and J. Cano, Multilayer graphene with a superlattice potential, *Phys. Rev. B* **107**, 195423 (2023).
- [69] D. Seleznev, J. Cano, and D. Vanderbilt, Inducing topological flat bands in bilayer graphene with electric and magnetic superlattices, *Phys. Rev. B* **110**, 205115 (2024).
- [70] B. T. Zhou, S. Egan, and M. Franz, Moiré flat chern bands and correlated quantum anomalous hall states generated by spin-orbit couplings in twisted homobilayer  $\text{MoS}_2$ , *Phys. Rev. Res.* **4**, L012032 (2022).
- [71] C. Wang, X. Shen, R. Guo, C. Wang, W. Duan, and Y. Xu, Fractional chern insulators in moiré flat bands with high chern numbers, *arXiv preprint arXiv:2408.03305* <https://doi.org/10.48550/arXiv.2408.03305> (2024).
- [72] H. Wang, Y. Fan, and H. Zhang, Electrically tunable high-chern-number quasiflat bands in twisted antiferromagnetic topological insulators, *Phys. Rev. B* **110**, 085135 (2024).
- [73] G. Chen, A. L. Sharpe, E. J. Fox, Y.-H. Zhang, S. Wang, L. Jiang, B. Lyu, H. Li, K. Watanabe, T. Taniguchi, *et al.*, Tunable correlated chern insulator and ferromagnetism in a moiré superlattice, *Nature* **579**, 56 (2020).
- [74] S. Chen, M. He, Y.-H. Zhang, V. Hsieh, Z. Fei, K. Watanabe, T. Taniguchi, D. H. Cobden, X. Xu, C. R. Dean, *et al.*, Electrically tunable correlated and topological states in twisted monolayer-bilayer graphene, *Nat. Phys.* **17**, 374 (2021).
- [75] L.-Q. Xia, S. C. de la Barrera, A. Uri, A. Sharpe, Y. H. Kwan, Z. Zhu, K. Watanabe, T. Taniguchi, D. Goldhaber-Gordon, L. Fu, *et al.*, Helical trilayer graphene: a moiré platform for strongly-interacting topological bands, *arXiv preprint arXiv:2310.12204* <https://doi.org/10.1038/s41567-024-02731-6> (2023).
- [76] H. Peng, J. Zhong, Q. Feng, Y. Hu, Q. Li, S. Zhang, J. Mao, J. Duan, and Y. Yao, Abundant electric-field tunable symmetry-broken states in twisted monolayer-bilayer graphene, *Commun. Phys.* **7**, 240 (2024).
- [77] J. Liu, Z. Ma, J. Gao, and X. Dai, Quantum valley hall effect, orbital magnetism, and anomalous hall effect in twisted multilayer graphene systems, *Phys. Rev. X* **9**, 031021 (2019).

- [78] P. J. Ledwith, A. Vishwanath, and E. Khalaf, Family of ideal chern flatbands with arbitrary chern number in chiral twisted graphene multilayers, *Phys. Rev. Lett.* **128**, 176404 (2022).
- [79] J. Wang and Z. Liu, Hierarchy of ideal flatbands in chiral twisted multilayer graphene models, *Phys. Rev. Lett.* **128**, 176403 (2022).
- [80] J. Dong, P. J. Ledwith, E. Khalaf, J. Y. Lee, and A. Vishwanath, Many-body ground states from decomposition of ideal higher chern bands: Applications to chirally twisted graphene multilayers, *Phys. Rev. Res.* **5**, 023166 (2023).
- [81] M. Yang, Flat bands and high chern numbers in twisted multilayer graphene, *J. Math. Phys.* **64**, <https://doi.org/10.1063/5.0153987> (2023).
- [82] S. Zhang, X. Dai, and J. Liu, Spin-polarized nematic order, quantum valley hall states, and field-tunable topological transitions in twisted multilayer graphene systems, *Phys. Rev. Lett.* **128**, 026403 (2022).
- [83] P. San-Jose, J. González, and F. Guinea, Non-abelian gauge potentials in graphene bilayers, *Phys. Rev. Lett.* **108**, 216802 (2012).
- [84] G. Tarnopolsky, A. J. Kruchkov, and A. Vishwanath, Origin of magic angles in twisted bilayer graphene, *Phys. Rev. Lett.* **122**, 106405 (2019).
- [85] R. Roy, Band geometry of fractional topological insulators, *Phys. Rev. B* **90**, 165139 (2014).
- [86] M. Claassen, C. H. Lee, R. Thomale, X.-L. Qi, and T. P. Devereaux, Position-momentum duality and fractional quantum hall effect in chern insulators, *Phys. Rev. Lett.* **114**, 236802 (2015).
- [87] P. J. Ledwith, G. Tarnopolsky, E. Khalaf, and A. Vishwanath, Fractional chern insulator states in twisted bilayer graphene: An analytical approach, *Phys. Rev. Res.* **2**, 023237 (2020).
- [88] J. Wang, J. Cano, A. J. Millis, Z. Liu, and B. Yang, Exact landau level description of geometry and interaction in a flatband, *Phys. Rev. Lett.* **127**, 246403 (2021).
- [89] R. Bistritzer and A. H. MacDonald, Moiré bands in twisted double-layer graphene, *Proc. Natl. Acad. Sci. U.S.A.* **108**, 12233 (2011).
- [90] J. M. B. Lopes dos Santos, N. M. R. Peres, and A. H. Castro Neto, Continuum model of the twisted graphene bilayer, *Phys. Rev. B* **86**, 155449 (2012).
- [91] M. S. Dresselhaus and G. Dresselhaus, Intercalation compounds of graphite, *Adv. Phys.* **30**, 139 (1981).
- [92] Y. Shi, S. Xu, Y. Yang, S. Slizovskiy, S. V. Morozov, S.-K. Son, S. Ozdemir, C. Mullan, J. Barrier, J. Yin, *et al.*, Electronic phase separation in multilayer rhombohedral graphite, *Nature* **584**, 210 (2020).
- [93] H. Zhou, T. Xie, A. Ghazaryan, T. Holder, J. R. Ehrets, E. M. Spanton, T. Taniguchi, K. Watanabe, E. Berg, M. Serbyn, *et al.*, Half-and quarter-metals in rhombohedral trilayer graphene, *Nature* **598**, 429 (2021).
- [94] M. Koshino, N. F. Q. Yuan, T. Koretsune, M. Ochi, K. Kuroki, and L. Fu, Maximally localized wannier orbitals and the extended hubbard model for twisted bilayer graphene, *Phys. Rev. X* **8**, 031087 (2018).
- [95] S. Lisi, X. Lu, T. Benschop, T. A. de Jong, P. Stepanov, J. R. Duran, F. Margot, I. Cucchi, E. Cappelli, A. Hunter, *et al.*, Observation of flat bands in twisted bilayer graphene, *Nat. Phys.* **17**, 189 (2021).
- [96] S. Carr, S. Fang, Z. Zhu, and E. Kaxiras, Exact continuum model for low-energy electronic states of twisted bilayer graphene, *Phys. Rev. Res.* **1**, 013001 (2019).
- [97] N. Leconte, S. Javvaji, J. An, A. Samudrala, and J. Jung, Relaxation effects in twisted bilayer graphene: A multiscale approach, *Phys. Rev. B* **106**, 115410 (2022).
- [98] Supplementary Material.
- [99] S. H. Aronson, T. Han, Z. Lu, Y. Yao, K. Watanabe, T. Taniguchi, L. Ju, and R. C. Ashoori, Displacement field-controlled fractional chern insulators and charge density waves in a graphene/hbn moiré superlattice, *arXiv preprint arXiv:2408.11220* <https://doi.org/10.48550/arXiv.2408.11220> (2024).
- [100] F. Wilczek and A. Zee, Appearance of gauge structure in simple dynamical systems, *Phys. Rev. Lett.* **52**, 2111 (1984).
- [101] A. K. Pati, Relation between “phases” and “distance” in quantum evolution, *Phys. Lett. A* **159**, 105 (1991).
- [102] T. Fukui, Y. Hatsugai, and H. Suzuki, Chern numbers in discretized brillouin zone: Efficient method of computing (spin) hall conductances, *J. Phys. Soc. Jpn.* **74**, 1674 (2005).
- [103] R. Cheng, Quantum geometric tensor (fubini-study metric) in simple quantum system: A pedagogical introduction, *arXiv preprint arXiv:1012.1337* <https://doi.org/10.48550/arXiv.1012.1337> (2010).
- [104] B. Mera and T. Ozawa, Engineering geometrically flat chern bands with fubini-study kähler structure, *Phys. Rev. B* **104**, 115160 (2021).
- [105] N. Mao, C. Xu, J. Li, T. Bao, P. Liu, Y. Xu, C. Felser, L. Fu, and Y. Zhang, Transfer learning relaxation, electronic structure and continuum model for twisted bilayer mote2, *Commun. Phys.* **7**, 262 (2024).
- [106] C. Huang, T. M. R. Wolf, W. Qin, N. Wei, I. V. Blinov, and A. H. MacDonald, Spin and orbital metallic magnetism in rhombohedral trilayer graphene, *Phys. Rev. B* **107**, L121405 (2023).
- [107] K. c. v. Kolář, Y. Zhang, S. Nadj-Perge, F. von Oppen, and C. Lewandowski, Electrostatic fate of  $n$ -layer moiré graphene, *Phys. Rev. B* **108**, 195148 (2023).
- [108] K. Kolář, D. Waters, J. Folk, M. Yankowitz, and C. Lewandowski, Single-gate tracking behavior in flat-band multilayer graphene devices, *arXiv e-prints*, [arXiv:2503.10749](https://arxiv.org/abs/2503.10749) (2025), [arXiv:2503.10749](https://arxiv.org/abs/2503.10749) [cond-mat.mes-hall].
- [109] M. Xie and A. H. MacDonald, Nature of the correlated insulator states in twisted bilayer graphene, *Phys. Rev. Lett.* **124**, 097601 (2020).
- [110] B. A. Bernevig, Z.-D. Song, N. Regnault, and B. Lian, Twisted bilayer graphene. iii. interacting hamiltonian and exact symmetries, *Phys. Rev. B* **103**, 205413 (2021).
- [111] D. Waters, R. Su, E. Thompson, A. Okounkova, E. Arreguin-Martinez, M. He, K. Hinds, K. Watanabe, T. Taniguchi, X. Xu, *et al.*, Topological flat bands in a family of multilayer graphene moiré lattices, *Nat. Comm.* **15**, 1 (2024).
- [112] L. M. Malard, J. Nilsson, D. C. Elias, J. C. Brant, F. Plentz, E. S. Alves, A. H. Castro Neto, and M. A. Pimenta, Probing the electronic structure of bilayer graphene by raman scattering, *Phys. Rev. B* **76**, 201401 (2007).
- [113] J. Jung and A. H. MacDonald, Accurate tight-binding models for the  $\pi$  bands of bilayer graphene, *Phys. Rev. B* **89**, 035405 (2014).